JACS
JOURNAL OF THE AMERICAN CHEMICAL SOCIETY

Communication

pubs.acs.org/JACS

Tension Sensing Nanoparticles for Mechano-Imaging at the Living/Nonliving Interface

Yang Liu, Kevin Yehl, Yoshie Narui, and Khalid Salaita*

Department of Chemistry, Emory University, 1515 Dickey Drive, Atlanta, Georgia, United States

Supporting Information

ABSTRACT: Studying chemomechanical coupling at interfaces is important for fields ranging from lubrication and tribology to microfluidics and cell biology. Several polymeric macro- and microscopic systems and cantilevers have been developed to image forces at interfaces, but few materials are amenable for molecular tension sensing. To address this issue, we have developed a gold nanoparticle sensor for molecular tension-based fluorescence microscopy. As a proof of concept, we imaged the tension exerted by integrin receptors at the interface between living cells and a substrate with high spatial (<1 μm) resolution, at 100 ms acquisition times and with molecular specificity. We report integrin tension values ranging from 1 to 15 pN and a mean of ∼1 pN within focal adhesions. Through the use of a conventional fluorescence microscope, this method demonstrates a force sensitivity that is 3 orders of magnitude greater than is achievable by traction force microscopy or polydimethylsiloxane micropost arrays,[1] which are the standard in cellular biomechanics.

One of the most significant challenges pertaining to understanding the interplay between mechanical forces and chemical reactions involves elucidating the magnitude of force experienced by specific molecules as a function of time and space.[2a−c] To address this need, several pioneering groups in the area of mechanochemistry have developed force-sensitive chromophores, or mechanophores, that respond to mechanical tension by undergoing covalent bond rearrangements that shift absorbance or fluorescence emission.[3] Nonetheless, given the relatively large changes in free energy required to break covalent bonds, current mechanophore probes are sensitive to forces in the range of hundreds to thousands of pN (∼10−100 kcal/mol, assuming a 10 Å displacement).[4] Thus, current mechanophores are unable to probe forces in the range of 1−50 pN that can drive conformational changes in macromolecules and molecular assemblies.

Tension-driven conformational rearrangements underpin many of the fundamental processes that regulate living systems. For example, cell division,[5] translation,[6] and transcription[7] require spatially and temporally coordinated low pN range forces to proceed. Accordingly, our group recently developed a method termed molecular tension-based fluorescence microscopy (MTFM), to measure pN forces exerted by cell surface receptors.[2b] MTFM employs a ligand molecule linked to a polymeric "spring" and anchored to a surface. The linker is flanked by a pair of dyes utilizing fluorescence resonance energy transfer (FRET) to report on molecular forces that extend the polymer from its resting position. MTFM offers the only method to visualize pN forces exerted between membrane receptors and their extracellular ligands.[2b] We rationalized that, by developing a gold nanoparticle (AuNP)-based mechanophore, the force sensitivity of MTFM could be extended to measure receptor tension magnitudes that are not practically accessible by FRET-based approaches, such as the genetically encoded spider silk construct,[2a] and our own FRET-based polyethylene glycol (PEG) tension sensors.[2b]

Noble metal nanoparticles (NPs) have revolutionized the field of chemical sensing due to their unique optical, electrical, electrochemical, and catalytic properties.[8] Moreover, the relatively biocompatible nature of AuNPs have lent itself to biological sensing applications for both *in vivo* and *in vitro* assays.[9] In many of these applications, the superior fluorescence quenching ability of AuNPs is exploited to achieve high sensitivity turn-on detection.[10] Compared to molecular quenchers, the effective quenching distance of AuNPs can be as long as several tens of nanometers.[11] Theoretical and experimental studies have shown that the distance-dependent quenching of 1−20 nm AuNPs follows a $1/r^4$ relationship, termed nanometal surface energy transfer (NSET),[12] which provides a highly sensitive approach to measuring molecular distances in living systems.[13]

Herein, we report on an AuNP-based sensor for MTFM to visualize the pN-range force dynamics of integrin receptors during cell adhesion (Scheme 1). As a proof of concept, we target the $\alpha_V\beta_3$ integrins using high-affinity peptides, because integrins are the primary molecules to sustain large tensile loads supporting cell adhesion and migration.[14] The AuNP MTFM sensor utilizes a calibrated NSET response to determine the molecular extension of an entropic polymer "spring"[15] anchored to the AuNP scaffold. This distance information is then used to infer the corresponding molecular tension. Thus, this probe provides the first reversible mechanosensor for imaging integrin molecular tension.

Scheme 1 describes the AuNP-MTFM approach. To synthesize the ligand (Figure S1), cyclic Arg-Gly-Asp-D-Phe-Lys-(Cys) peptide (cRGDfK(C)) was first modified with an NHS-azide in high yield (>90%). This afforded the orthogonal reactive thiol and azide groups for further modification. Maleimide-Alexa488 dye and alkyne-terminated PEG (MW 3400) were further coupled to the thiol and azide, respectively.

Received: February 15, 2013

   dx.doi.org/10.1021/ja401494e | J. Am. Chem. Soc. XXXX, XXX, XXX−XXX

Scheme 1. AuNP-Based Molecular Tension Fluorescence Microscopy (AuNP-MTFM)

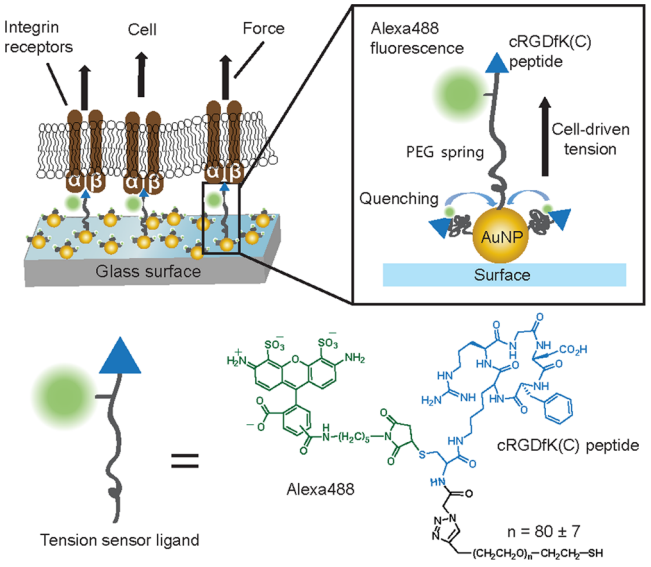

The purity of the final product was confirmed by HPLC and MALDI-TOF MS (Figure S2). The mass distribution of the PEG polymer indicated a contour length of 28.0 ± 2.5 nm, assuming a monomer length of 0.35 nm.[16] Based on the worm-like chain (WLC) model for force-induced molecular extension,[17] the fluorophore should rest at 4.9 ± 0.2 nm from the AuNP surface at low packing density (<29 molecules/AuNP) and can be extended up to ~28 nm away from the Au surface. Thus, the sensor should generate a 10-fold increase in fluorescence signal, if subjected to sufficient tension.

To quantify the distance between the Alexa488 dye and the AuNP surface, we measured the d_0 (distance at which the quenching efficiency = 0.5) by using highly packed duplex DNA as a molecular ruler. Briefly, a series of DNA duplexes conjugated with 5′ Alexa488 at the terminus of one strand and a 5′ thiol at the terminus of the complementary strand were immobilized to the AuNP surface, while the salt concentration was titrated to 0.3 M NaCl (Figure 1a,b). To minimize self-quenching, the dye-labeled DNA duplex was diluted in a 1:9 ratio using identical duplexes that lacked the 5′ fluorophore. We used the OliGreen assay and the calibrated fluorescence intensity to provide two independent methods to determine the DNA loading number per particle, as reported in Figure 1b and Table S1.[18] These values suggest that the duplexes present orientations perpendicular to the Au surface.[19] We then measured the fluorescence intensity of the four AuNP-dsDNA-Alexa488 conjugates before and after dissolution of the AuNP. The quenching efficiency of triplicate AuNP samples was plotted as a function of distance and fit to the NSET equation (Figure 1c), providing a d_0 of 13.6 ± 0.3 nm. This value is in agreement with literature precedents that reported d_0 of 10.4 and 15.7 nm for 10 nm AuNPs displaying Atto647, and Cy3, respectively.[11,20] Importantly, we can combine this calibrated NSET equation and the WLC relation, which has been experimentally and theoretically validated for PEG, to generate a theoretical curve depicting quenching efficiency as a function of applied tension (Figure 1d). Based on this plot, the quenching efficiency decreases from 0.9 to 0.1 when a force of 25 pN is applied, affording a wider dynamic range than our reported FRET-based PEG tension sensor,[2b] and a 5- to

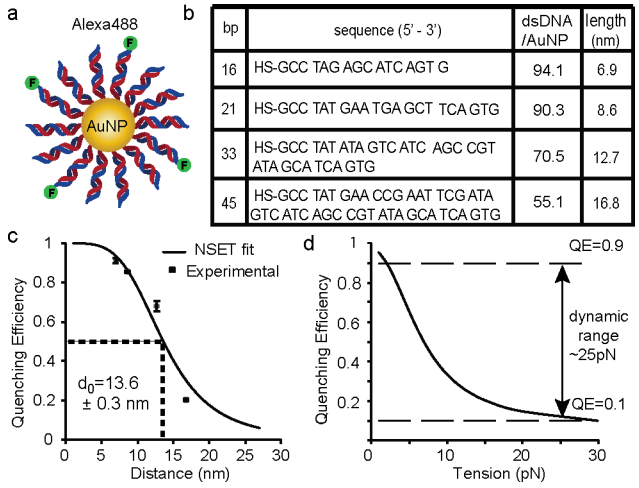

bp	sequence (5′ - 3′)	dsDNA /AuNP	length (nm)
16	HS-GCC TAG AGC ATC AGT G	94.1	6.9
21	HS-GCC TAT GAA TGA GCT TCA GTG	90.3	8.6
33	HS-GCC TAT ATA GTC ATC AGC CGT ATA GCA TCA GTG	70.5	12.7
45	HS-GCC TAT GAA CCG AAT TCG ATA GTC ATC AGC CGT ATA GCA TCA GTG	55.1	16.8

Figure 1. NSET calibration. (a) To determine d_0, particles were functionalized with a binary mixture of 1:9 labeled:unlabeled dsDNA. (b) Table showing DNA sequences used, their measured density, and predicted lengths. (c) Plot showing quenching efficiency as a function of distance from AuNP surface. Data were fitted to NSET model and d_0 was determined to be 13.6 ± 0.3 nm. (d) Theoretical force-quenching efficiency plot based on combining WLC and NSET models. Force dynamic range corresponds to quenching efficiency ranging from 0.9 to 0.1.

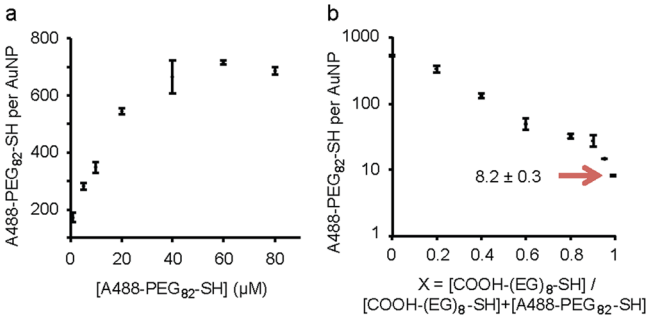

Figure 2. PEG conformation on AuNP surface. Plot of A488-PEG_{82}-SH loading as a function of incubation with single ligand (a) and binary mixture of ligands of A488-PEG_{82}-SH and COOH-EG_8-SH (b). Total ligand concentration was maintained at 40 μM, and ratio was varied from 0 to 0.99.

10-fold improvement in signal-to-background when compared to the genetically encoded spider-silk tension sensor constructs.[2a,c]

Given that ligand density dictates its conformation on the AuNP surface[21] and consequently influences sensor response, we quantified the ligand density as function of its incubation concentration. We found that the number of surface bound ligands per AuNP ranges from 100 to 700 when ligand concentration was varied from 1 μM to 80 μM (Figure 2a). To passivate the bare Au surface and increase particle stability, we introduced other competing thiolated ethylene glycol molecules to form binary PEG-coated AuNPs. Among these, we found that COOH-EG_8-SH to be advantageous due to increased particle stability. The dual PEG modification strategy offered significant improvement in controlling the number of ligand molecules per particle, especially at low ligand densities, e.g., 1−10 ligands per NP (Figure 2b). This ensured that the polymers adopt their predicted Flory radius of 4.9 nm, thus maintaining the relaxed mushroom conformation and generating a more reproducible response.[16]

dx.doi.org/10.1021/ja401494e | J. Am. Chem. Soc. XXXX, XXX, XXX−XXX

We next verified the conformation of the polymer for particles displaying 8.2 ± 0.3 Alexa488-PEG_{82}-SH per NP. Using the measured d_0 of 13.6 nm, the quenching efficiency data (Figure S3) indicated that the dye was 8.4 nm from the NP surface. This distance is in general agreement with the predicted dye-AuNP distance of 7.4 nm, which is the sum of the expected contour length of COOH-EG_8-SH (2.8 nm)[22] and the Flory radius of the partially crowded Alexa488-PEG_{82}-SH (4.6 nm). We further verified the PEG conformation using negative staining TEM of samples with different surface loading densities (Figure S4).

Typically, AuNPs are immobilized to a substrate using primary amines or thiols, which provide sufficient binding for most chemical sensing applications. However, to measure molecular forces, we needed to irreversibly immobilize AuNP conjugates, such that particles would not translocate in response to external tension (Figure S5). Therefore, we used lipoic acid ligands to provide strong affinity to the Au surface due to multivalent binding.[23] Moreover, this method allowed immobilization of AuNP-based MTFM sensors within a few minutes, thus minimizing the aggregation due to extended incubation times. To generate these surfaces, amine-functionalized substrates were reacted with a mixture of 5% w/v mPEG-NHS (MW 2000) and 0.5% w/v lipoic acid-PEG-NHS (MW 3400) in 0.1 M sodium bicarbonate buffer, overnight. AFM was used to determine the surface density of anchored AuNPs (Figure 3a) and showed that the average interparticle distance was ∼110 nm. Although particle spacing was disordered across the substrate, this type of packing is known to allow cell focal adhesion formation.[24]

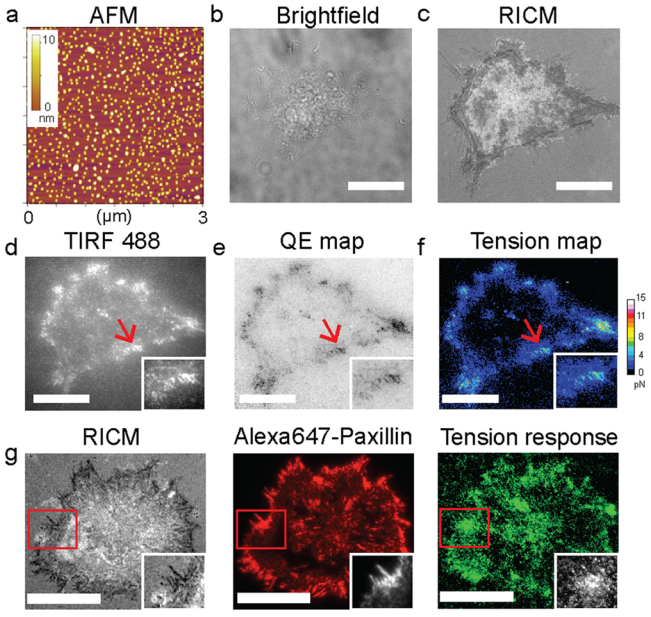

Figure 3. Mechano-imaging of integrins in live cell. (a) AFM image showing the typical AuNP sensor distribution. After 1 h of cell culture on the sensor surface, brightfield (b) and RICM (c) images were captured to visualize cell adhesion. RICM (c) clearly revealed adhesion sites (dark region) mostly at the cell edge. (d) TIRF image (500 ms acquisition time) of the same cell shown in (b,c). Raw fluorescence data were converted to a quenching efficiency map using bulk quenching efficiency of AuNP sensor. A force map was then calculated using the WLC model. Inset shows rod-like focal adhesions with a high level of force. Scale bar, 20 μm. (g) Representative images showing that paxillin colocalizes with tension signals within focal adhesions. Scale bar, 15 μm.

To image the tension exerted by living cells, human breast cancer cells (HCC 1143) were plated onto the AuNP sensor-modified glass surfaces for 1 h to allow the cells to form adhesions. To minimize autofluorescence and maximize signal to background ratio, we performed total internal reflection fluorescence microscopy using a laser coupled inverted microscope. At the resting state, we observed relatively low and uniform background fluorescence intensity (Figure S5c). After cells adhered and polarized on the surface, we used brightfield (Figure 3b) and reflection interference contrast microscopy (RICM, Figure 3c) to observe the binding between the cell and the surface. In the AuNP-MTFM channel (TIRF 488), we observed a strong fluorescence intensity increase (up to 7 fold over background) (Figure 3d) that was strongly associated with the cell-binding pattern in RICM (Figure 3c). The signal to background ratio at the brightest spots of the image was ∼20, which allowed direct and facile identification of areas of high tension. In some local regions, rod-like contact patterns formed (Figure 3d–f, red arrow, inset), suggesting formation of mature focal adhesions.[25] Using the bulk quenching efficiency values and the NSET model, we first determined the average PEG extension at each pixel of the image (Figure S7). Next, the WLC model was used to estimate the minimum ensemble tension exerted at each sensor ligand, thus providing a tension map (Figure 3f). While many techniques, such as traction force microscopy and polydimethylsiloxane (PDMS) post arrays, have been used to measure cell forces, our method detects pN tension, thus representing a 3-order of magnitude sensitivity improvement and is exclusive to RGD-binding receptor molecules. Temporal and spatial resolution of MTFM are not different from standard fluorescence microscopy techniques, which exceed that of traction force microscopy and especially if combined with super-resolution imaging or single-molecule imaging approaches.[26]

To validate that the tension signal is due to specific focal adhesion complexes, cells were cultured onto passivated PEG-only surfaces or nonsensing AuNP conjugate surfaces. Minimal cell attachment was observed under our experimental conditions, thus showing specificity of RGD binding (Figure S7). In another experiment, we treated cells on AuNP-MTFM sensor surfaces with 25 μM latrunculin B (LatB), which inhibits actin polymerization and thus prevents force generation (Figure S8). After 10 min of treatment with LatB, the increased fluorescence completely dissipated and returned to background levels for all observed cells (Figure S8). In addition, we immunostained for paxillin, a marker of focal adhesions (see Methods in SI). Figure 3g shows a high degree of overlap between AuNP-MTFM response and paxillin staining. Note that the tension signal significantly weakens once cells are fixed, likely due to nm scale cytoskeletal and PEG relaxation. Taken together, these experiments clearly show that the reversible fluorescence response is due to mechanical tension exerted by integrins on the MTFM sensor.

To demonstrate dynamic imaging capabilities, we collected time-lapse images of a cell as it contacted a substrate and initiated focal adhesion formation (Figure 4, SI movie). The tension signal rapidly translocated from the center of the cell to its periphery over the span of 10 min. This is the first direct evidence showing the presence of integrin tension during initial cell substrate contact, which was previously inferred by ligand translocation.[27] In another time-lapse video, we captured the tension dynamics of the reverse event, as a cell underwent contraction and high-tension regions at the cell periphery dissipated (Figure S9, SI

dx.doi.org/10.1021/ja401494e | J. Am. Chem. Soc. XXXX, XXX, XXX−XXX

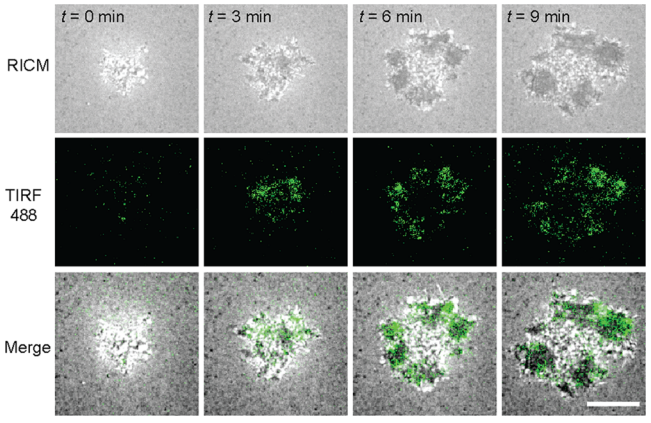

Figure 4. Initial tension dynamics during cell adhesion. Time-lapse images recording the first 10 min of cell-substrate interactions after the cell engaged the surface. Tension signal (TIRF 488 channel, 100 ms acquisition time) colocalized with cell binding locations as shown in the RICM channel. Scale bar, 15 μm.

movie). The alignments of tension signals are clearly perpendicular to the cell edge, corresponding to its distal orientation.[25] Finally, histogram analysis of force distribution within focal adhesions showed a mean tension of ~1.0 pN, which is in agreement with estimates from traction force microscopy and PDMS post arrays (Figure S10). Interestingly, some regions displayed tension values that are an order of magnitude greater than the average, which is compatible with integrin-RGD rupture forces measured using AFM.[28]

In summary, we report the first NP-based molecular tension probe and use it to image the dynamics of integrin adhesions. We calibrated the NSET response and verified the sensor conformation on the AuNP surface. In principle, this sensor reports on molecular tension with a wider dynamic range than is fundamentally allowed by FRET-based methods. Note that the stability of the thiol Au bond exceeds that of integrin-RGD interaction, and thus the MTFM sensor is stable within our experimental conditions.[29] Surprisingly, we observed a wide distribution of tension magnitudes within adhesions. Given that NPs can be spatially patterned onto surfaces, this suggests that one may be able to readily investigate the role of ligand density and topology on force transmission. AuNPs can also be tracked using label-free methods, which should allow for dual force-localization studies in 3D.

■ ASSOCIATED CONTENT

Supporting Information

Supporting Information and movies. This material is available free of charge via the Internet at http://pubs.acs.org.

■ AUTHOR INFORMATION

Corresponding Author

k.salaita@emory.edu

Notes

The authors declare no competing financial interest.

■ ACKNOWLEDGMENTS

K.S. is grateful for support from the NIH (R01-GM097399), the Alfred P. Sloan Research Fellowship, and the Army Research Office (62570EGII). We thank Daniel Stabley for the TOC graphic design. AFM was performed with the support of Dr. Zheng Liu and Prof. Tianquan Lian at Emory. TEM was performed with the help of Chunfu Xu at the Robert P. Apkarian Integrated Electron Microscopy Core of Emory University.

■ REFERENCES

(1) Legant, W. R.; Choi, C. K.; Miller, J. S.; Shao, L.; Gao, L.; Betzig, E.; Chen, C. S. *Proc. Natl. Acad. Sci. U.S.A.* **2013**, *110*, 881.
(2) (a) Grashoff, C.; Hoffman, B. D.; Brenner, M. D.; Zhou, R.; Parsons, M.; Yang, M. T.; McLean, M. A.; Sligar, S. G.; Chen, C. S.; Ha, T.; Schwartz, M. A. *Nature* **2010**, *466*, 263. (b) Stabley, D. R.; Jurchenko, C.; Marshall, S. S.; Salaita, K. S. *Nat. Methods* **2012**, *9*, 64. (c) Borghi, N.; Sorokina, M.; Shcherbakova, O. G.; Weis, W. I.; Pruitt, B. L.; Nelson, W. J.; Dunn, A. R. *Proc. Natl. Acad. Sci. U.S.A.* **2012**, *109*, 12568.
(3) Caruso, M. M.; Davis, D. A.; Shen, Q.; Odom, S. A.; Sottos, N. R.; White, S. R.; Moore, J. S. *Chem. Rev.* **2009**, *109*, 5755.
(4) Kryger, M. J.; Munaretto, A. M.; Moore, J. S. *J. Am. Chem. Soc.* **2011**, *133*, 18992.
(5) Fink, J.; Carpi, N.; Betz, T.; Bétard, A.; Chebah, M.; Azioune, A.; Bornens, M.; Sykes, C.; Fetler, L.; Cuvelier, D.; Piel, M. *Nat. Cell Biol.* **2011**, *13*, 771.
(6) Chicurel, M. E.; Singer, R. H.; Meyer, C. J.; Ingber, D. E. *Nature* **1998**, *392*, 730.
(7) Yin, H.; Wang, M. D.; Svoboda, K.; Landick, R.; Block, S. M.; Gelles, J. *Science* **1995**, *270*, 1653.
(8) Saha, K.; Agasti, S. S.; Kim, C.; Li, X.; Rotello, V. M. *Chem. Rev.* **2012**, *112*, 2739.
(9) Murphy, C. J.; Gole, A. M.; Stone, J. W.; Sisco, P. N.; Alkilany, A. M.; Goldsmith, E. C.; Baxter, S. C. *Acc. Chem. Res.* **2008**, *41*, 1721.
(10) Dubertret, B.; Calame, M.; Libchaber, A. J. *Nat. Biotechnol.* **2001**, *19*, 365.
(11) Chhabra, R.; Sharma, J.; Wang, H.; Zou, S.; Lin, S.; Yan, H.; Lindsay, S.; Liu, Y. *Nanotechnology* **2009**, *20*, 485201.
(12) Yun, C.; Javier, A.; Jennings, T.; Fisher, M.; Hira, S.; Peterson, S.; Hopkins, B.; Reich, N.; Strouse, G. *J. Am. Chem. Soc.* **2005**, *127*, 3115.
(13) Chen, Y.; O'Donoghue, M. B.; Huang, Y. F.; Kang, H.; Phillips, J. A.; Chen, X.; Estevez, M. C.; Yang, C. J.; Tan, W. *J. Am. Chem. Soc.* **2010**, *132*, 16559.
(14) Pfaff, M.; Tangemann, K.; Müller, B.; Gurrath, M.; Müller, G.; Kessler, H.; Timpl, R.; Engel, J. *J. Biol. Chem.* **1994**, *269*, 20233.
(15) Shroff, H.; Reinhard, B. M.; Siu, M.; Agarwal, H.; Spakowitz, A.; Liphardt, J. *Nano Lett.* **2005**, *5*, 1509.
(16) De Gennes, P. *Macromolecules* **1980**, *13*, 1069.
(17) Bouchiat, C.; Wang, M.; Allemand, J. F.; Strick, T.; Block, S.; Croquette, V. *Biophys. J.* **1999**, *76*, 409.
(18) Yehl, K.; Joshi, J. P.; Greene, B. L.; Dyer, R. B.; Nahta, R.; Salaita, K. *ACS Nano* **2012**, *6*, 9150.
(19) Dulkeith, E.; Ringler, M.; Klar, T.; Feldmann, J.; Javier, A. M.; Parak, W. *Nano Lett.* **2005**, *5*, 585.
(20) Acuna, G. P.; Bucher, M.; Stein, I. H.; Steinhauer, C.; Kuzyk, A.; Holzmeister, P.; Schreiber, R.; Moroz, A.; Stefani, F. D.; Liedl, T.; Simmel, F. C.; Tinnefeld, P. *ACS Nano* **2012**, *6*, 3189.
(21) Levin, C. S.; Bishnoi, S. W.; Grady, N. K.; Halas, N. J. *Anal. Chem.* **2006**, *78*, 3277.
(22) Harder, P.; Grunze, M.; Dahint, R.; Whitesides, G.; Laibinis, P. *J. Phys. Chem. B* **1998**, *102*, 426.
(23) Mei, B. C.; Susumu, K.; Medintz, I. L.; Mattoussi, H. *Nat. Protoc.* **2009**, *4*, 412.
(24) Huang, J.; Gräter, S. V.; Corbellini, F.; Rinck-Jahnke, S.; Bock, E.; Kemkemer, R.; Kessler, H.; Ding, J.; Spatz, J. P. *Nano Lett.* **2009**, *9*, 1111.
(25) Gardel, M. L.; Schneider, I. C.; Aratyn-Schaus, Y.; Waterman, C. M. *Annu. Rev. Cell Dev. Biol.* **2010**, *26*, 315.
(26) Muzzey, D.; van Oudenaarden, A. *Annu. Rev. Cell Dev. Biol.* **2009**, *25*, 301.
(27) Yu, C.; Law, J. B. K.; Suryana, M.; Low, H. Y.; Sheetz, M. P. *Proc. Natl. Acad. Sci. U. S. A.* **2011**, *108*, 20585.
(28) Lehenkari, P. P.; Horton, M. A. *Biochem. Biophys. Res. Commun.* **1999**, *259*, 645.
(29) Grandbois, M.; Beyer, M.; Rief, M.; Clausen-Schaumann, H.; Gaub, H. E. *Science* **1999**, *283*, 1727.